PHILOSOPHICAL MAGAZINE B, 1990, VOL. 62, NO. 6, 615–645

Coarsening in the two-dimensional soap froth and the large-Q Potts model: a detailed comparison

By JAMES A. GLAZIER†

James Franck Institute and Department of Physics, University of Chicago, 5640 S. Ellis Avenue, Chicago, Illinois 60637, U.S.A.

MICHAEL P. ANDERSON and GARY S. GREST

Corporate Research Science Laboratory, Exxon Research and Engineering Company, Annadale, New Jersey 08801, U.S.A.

[*Received 29 August 1989‡ and accepted 19 January 1990*]

ABSTRACT

A detailed comparison between the experimental evolution of a two-dimensional soap froth and a next-nearest-neighbour $Q=\infty$ Potts model on a square lattice starting from identical initial conditions is presented. We compare the pattern evolution, dynamics, distribution functions and correlations of the two systems. We also examine in detail the relation between number of sides and area (Lewis' law) and two measures of pattern disorder. Overall agreement is found between the model and simulation, with a few systematic deviations which suggest that side redistribution is affected by subtle anisotropy and equilibration effects.

§1. INTRODUCTION

Two-dimensional coarsening occurs in a wide variety of materials, ranging from metal films to lipid monolayers and magnetic bubbles. In all such systems, surface-energy-driven diffusion leads to the motion of curved boundary walls causing certain cells to grow while others shrink and disappear. The result is a gradual increase in the overall length scale of the pattern. These basic dynamics interact with the geometrical constraint that vertices are threefold connected to produce a family of typical patterns of coordination number three. A typical coarsening process begins with a nearly regular array of hexagonal bubbles and gradually evolves into a completely disordered pattern with time-invariant distributions of the number of sides per bubble and bubble areas (a *scaling state*). Besides the intrinsic interest of the transition from order to disorder, coarsening has many technological applications in metallurgy, for example in the design of materials with particular mechanical properties. The coarsening properties of metals have therefore been widely studied (Beck 1954, Atkinson 1988). Unfortunately, in many cases, secondary effects such as impurity segregation and crystalline anisotropy mask the underlying universal features of two-dimensional coarsening.

To try to sort out the underlying ideal coarsening behaviour, we turn to the two-dimensional soap froth which was first proposed by Smith (1952) as a particularly

† Present address: AT&T Bell Laboratories, 600 Mountain Avenue, Murray Hill, New Jersey 07974, U.S.A.

‡ Received in final form 12 December 1989.

simple example of a cellular system which coarsens in time. In spite of a few discrepancies (Stavans and Glazier 1989) it appears that soap froths obey a simple dynamical law (von Neumann's (1952) law) for the evolution of bubbles:

$$\frac{da_n}{dt} = \kappa(n-6),$$

where a_n is the area of an n-sided bubble and κ is a system-dependent diffusion constant (Fu 1986, Glazier, Gross and Stavans 1987, Glazier and Stavans 1989). If von Neumann's law were all there were to froth evolution, the problem would be trivial; however, when bubbles disappear, their neighbours gain or lose sides, resulting in continual changes in each bubble's rate of growth or shrinkage. The difficulty in most models is to treat the redistribution of sides correctly.

There have been many approaches to modelling the evolution and scaling state of the soap froth. Examples include statistical mechanical and 'maximum-entropy' arguments (Rivier 1983, 1985, Mullins 1986, 1988, de Almeida and Iglesias 1988), vertex and boundary dynamics models (Fullman 1952, Weaire and Kermode 1983a, b, Frost and Thompson 1986, 1987, Kawasaki and Enomoto 1988, Kawasaki, Nagai and Nakasima 1989), mean-field theories (Marder 1987, Beenakker 1986, 1987, 1988, Fradkov 1988, Fradkov, Kravchenko and Shvindlerman 1985a, Fradkov, Shvindlerman and Udler 1985b, 1987) and Potts-model-type simulations (Anderson, Srolovitz, Grest and Sahni 1984, Srolovitz, Anderson, Sahni and Grest 1984b, Anderson 1986, Grest, Anderson and Srolovitz 1986, Grest, Srolovitz and Anderson 1988, Wejchert, Weaire and Kermode 1986, Weaire and Wejchert 1986). For a complete discussion of the various soap froth and grain growth models see the Ph.D Thesis of Glazier (1989).

Vertex and boundary dynamics models arise naturally from a consideration of the basic physics of a soap froth, in which gas diffuses across well defined soap films. The Potts model simulation, on the other hand, takes a quasi-microscopic metallurgical view of coarsening in which the interior of a grain is composed of a lattice of 'atoms' and the grain boundaries are the interface between different types (or orientations) of those 'atoms'. As in real coarsening, curvature of domain boundaries leads to increased wall energy on the convex side and hence to wall migration (fig. 1). Coarsening results because few-sided grains have larger total curvatures than many-sided grains and hence shrink.

The Potts model is space filling, unlike vertex models, and trades the deterministic diffusion of gas across a soap film for the probabilistic motion of an interface between domains of differing spin types. However, Grest *et al.* (1988) have shown numerically that the $Q=\infty$ state Potts model obeys von Neumann's law on average. If the redistribution of sides in the model is similar to that in an actual froth, we expect good agreement between the temporal evolution of the two systems. In this paper we examine precisely how good this assumption of identity is.

One difference between the Potts model and a real soap froth is the Potts model's orientationally anisotropic boundary energy. We show the anisotropy in a Wulff plot (fig. 2) at $T=0$ for three different ranges of interaction. The effect of the anisotropy is to absorb wall curvature at vertices and hence to reduce the effective force driving boundary motion. In the case of the nearest-neighbour square lattice (fig. 2 (*a*)), the anisotropy is so strong that the boundary walls flatten, and coarsening rapidly slows and stops (Anderson *et al.* 1984, 1986). We therefore work with the nearest-neighbour hexagonal (fig. 2 (*b*)) and next-nearest-neighbour square lattices (fig. 2 (*c*)) which have

Fig. 1

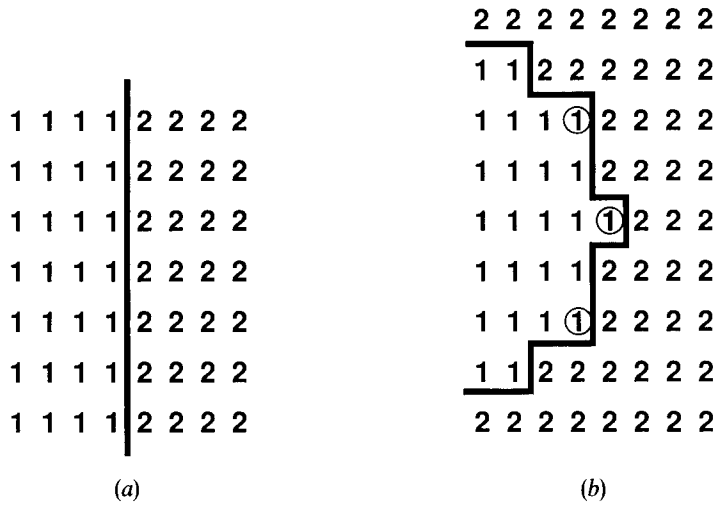

(*a*) (*b*)

Potts model grain–boundary migration. (*a*) Flat boundary, second-nearest-neighbour interaction. All boundary spins have energy 3; flips would increase energy to 5. (*b*) Curved boundary. Circled spins lose energy by flipping (5→3). The 2 grain will grow at the expense of the 1 grain.

Fig. 2

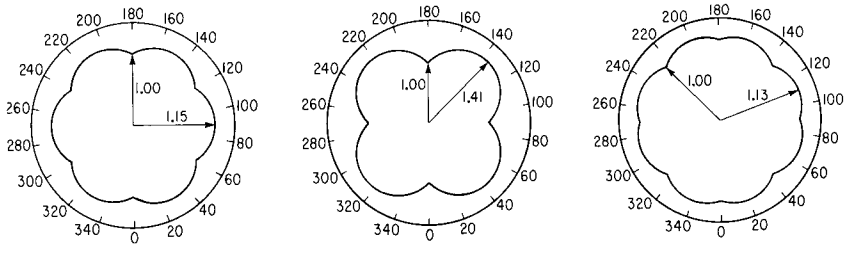

(*a*) (*b*) (*c*)

Potts model anisotropies. Energy per unit surface length as a function of surface angle (*a*) for a nearest-neighbour hexagonal lattice (from Srolovitz, Anderson, Grest and Sahni (1983)), (*b*) for a nearest-neighbour square lattice and (*c*) for a next-nearest-neighbour square lattice. The labelled arrows show energy extrema and values.

lower anisotropy. Anisotropy-related kinetic effects are common in metals (Beck 1954); so the tunable anisotropy of the Potts model can be an advantage in the study of metallic grain growth. Another difference between the froth and the Potts model is that the diffusion time of gas across a soap film is much slower than the equilibration time of the film along its length, while in the Potts model and most metals the two times are the same. Thus, soap films are closer in shape to true equilibrium surfaces than are grain boundaries in the Potts model and metals. In this respect our model differs significantly from that of Wejchert *et al.* (1986), who used a double time step, first applying von Neuman's law to fix target areas for each grain and then using Potts model evolution to relax the grain boundaries to an equilibrium configuration.

Compared with the many other models for two-dimensional coarsening, the Potts model has several significant advantages. Foremost is its simplicity. Its one assumption

is that wall energy is the only mechanism driving coarsening. There are no free parameters. Redistribution of sides on bubble disappearance occurs automatically without making further assumptions. Side swapping without disappearance (the $T1$ process) is also automatically included at the correct rate. In most other models the rate of $T1$ processes is included as a fitting parameter. Secondly, the Potts model can be easily extended to include grain coalescence and wall breakage. If instead of assigning a different spin to each grain, a fixed number Q of spins is used, then the probability of a broken wall between two grains which meet as a result of a reorganization of the lattice is just $1/Q$. Thus one can study in detail the effects of wall breakage on froth evolution (Anderson *et al.* 1984, Srolovitz *et al.* 1984b). Other straightforward extensions include three-dimensional lattices (limited by the availability of computer time to systems of size 100^3–140^3) (Anderson *et al.* 1989), the consideration of pinning centres (Srolovitz, Anderson, Grest and Sahni 1984a), orientational anisotropies (Grest, Srolovitz and Anderson 1985), and anomalous grain growth in which volume-dependent terms are added to the surface energy in the Hamiltonian (Srolovitz, Grest and Anderson 1985).

In this paper we present a detailed comparison between the evolution of two-dimensional soap froth and a large-Q, Q state Potts model simulation which begins with the same initial conditions. We compare dynamics, area and number of side distributions, as well as correlation functions for the two systems, and find generally good agreement. We speculate briefly on the roles of anisotropy and equilibration in pattern formation. A few alternative measures for the disorder of cellular patterns are also discussed.

§ 2. Experimental procedure

We have described the apparatus and experimental procedure elsewhere (Glazier *et al.* 1987). Most of the data discussed in this paper came from a cell 8·5 in × 11·5 in × $\frac{1}{8}$ in, using air as the working gas. We chose a larger cell size than that used in our earlier work to reduce the thickening of the Plateau borders in the sealed cell, which we have suggested as a possible cause for the anomalous power-law growth that we have previously observed in the soap froth (Stavans and Glazier 1989, Glazier and Stavans 1989). The simple experimental procedure was unchanged. We filled the cell with a well ordered array of small bubbles (typically 10000 bubbles at the start of experiment), placed it level on a photocopier and photocopied it periodically. The photocopier used in these runs (a Mitra model DC-1255) was a scanning type which heated the cell significantly during each copy. While the duration of heating was short and thus should not have significantly affected the dynamics of the froth, it did result in occasional wall breakage. The total numbers of walls broken during a run represented less than 0·1% of the total side redistribution but nevertheless may have resulted in slightly greater numbers of very-many-sided bubbles.

For image analysis, we selected 30 images from the experimental run, beginning at the beginning of the run and ending with the end of the experimetal data. We digitized a consistently chosen 30% sample of the image area using an IBAS digitizer with a resolution of 600 × 500 pixels in a square lattice. We then edited the digitized image by hand to remove obvious defects in the digitization and converted it into grains using a standard 'worm' technique, each pixel being assigned to a separately numbered grain for analysis. The image quality was sufficiently good that we had very few spurious bubbles or broken lines (fewer than 2%). We did occasionally have to edit the final distributions to remove spurious many- and few-sided bubbles caused by defects in digitization. The resolution of the digitizer was sufficient to represent a few thousand

bubbles with a typical size of 10×10 pixels. One advantage of this type of digitization was that the digitized images could serve directly as initial conditions for a square-lattice Potts model simulation, one pixel in the image corresponding to one spin in the model. A disadvantage was that the relatively small image area gave rather poor statistics at long times.

§ 3. The Potts model

We have mentioned that the basic driving force in a coarsening system is surface tension (or more generally surface energy) which creates pressure differences which result in gas diffusion. The Potts model puts surface tension on a lattice by defining an energy which is proportional to the total length of grain boundary in the system.

Mathematically we may do this by defining, on each site of our lattice, a spin $\sigma(i,j)$, where all the lattice points lying within a given grain in our initial configuration are assigned the same value of spin, with a different spin for each grain. To increase computational efficiency, we may re-use spins, employing a finite number Q of spins, while taking Q large enough that the probability of two grains with like spins coming into contact and coalescing is small. The energy of interaction between like spins is defined to be zero, and between unlike spins to be one. We may thus write the total Hamiltonian for our spin system as

$$H = -\sum_{i,j} \sum_{\substack{\text{neighbours} \\ i',j'}} \delta_{\sigma(i,j),\sigma(i',j')} - 1, \tag{1}$$

where the range of the second sum will affect the nature of the interaction. The spins are flipped using a Monte Carlo selection, where a spin is chosen at random and flipped only if the flip would lower the system energy. This corresponds to the zero-temperature limit, which is appropriate if we want to study relaxation processes rather than phase transitions. The temperature remains a useful control parameter, however, for the analysis of conditions where fluctuations are significant.

We may understand why this surface energy results in a von Neumann-like diffusion if we look closely at a region of grain boundary with a next-nearest-neighbour square-lattice interaction (fig. 1). If the boundary is straight (fig. 1(*a*)) there is no tendency for spins to flip, since all spins border more of their own kind than of other kinds. If the boundary is curved (fig. 1 (*b*)), spins on the convex side will tend to see more of the opposing type and thus to flip. The result is that the boundary recedes at a rate proportional to its curvature. The original version of this argument was given by Plateau (1843, 1873) in his study of soap bubbles. Since the system attempts to minimize surface length, the stable geometrical configuration is composed of three films meeting at 120° (fig. 3), and von Neumann's (1952) original derivation of his law follows. If we characterize coarsening by fitting the average area $\langle a \rangle$ per bubble as a function of time to a power law

$$\langle a \rangle \propto t^{\alpha}, \tag{2}$$

we obtain a growth exponent characterizing the coarsening. It is straightforward to show that any coarsening system which obeys von Neumann's law and is in a scaling state must have $\alpha = 1$ (von Neumann 1952, Mullins 1956, 1986, Marder 1987).

One difficulty with the Potts model is that a simple nearest-neighbour interaction on a square lattice results in a strongly anisotropic surface energy (the ratio of lowest to highest surface energies as a function of orientation is 1·41) which allows stable vertices

Fig. 3

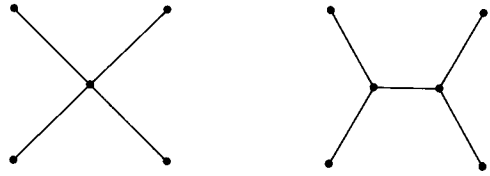

(*a*) (*b*)

Length minimization and coordination number. The relative length of sides of four vertices connected by (*a*) four lines running to a single 90° vertex (length, 2·828) and (*b*) five lines running to two 120° vertices (length, 2·732). Since surface tension tends to minimize side length, (*a*) decays into (*b*).

Fig. 4

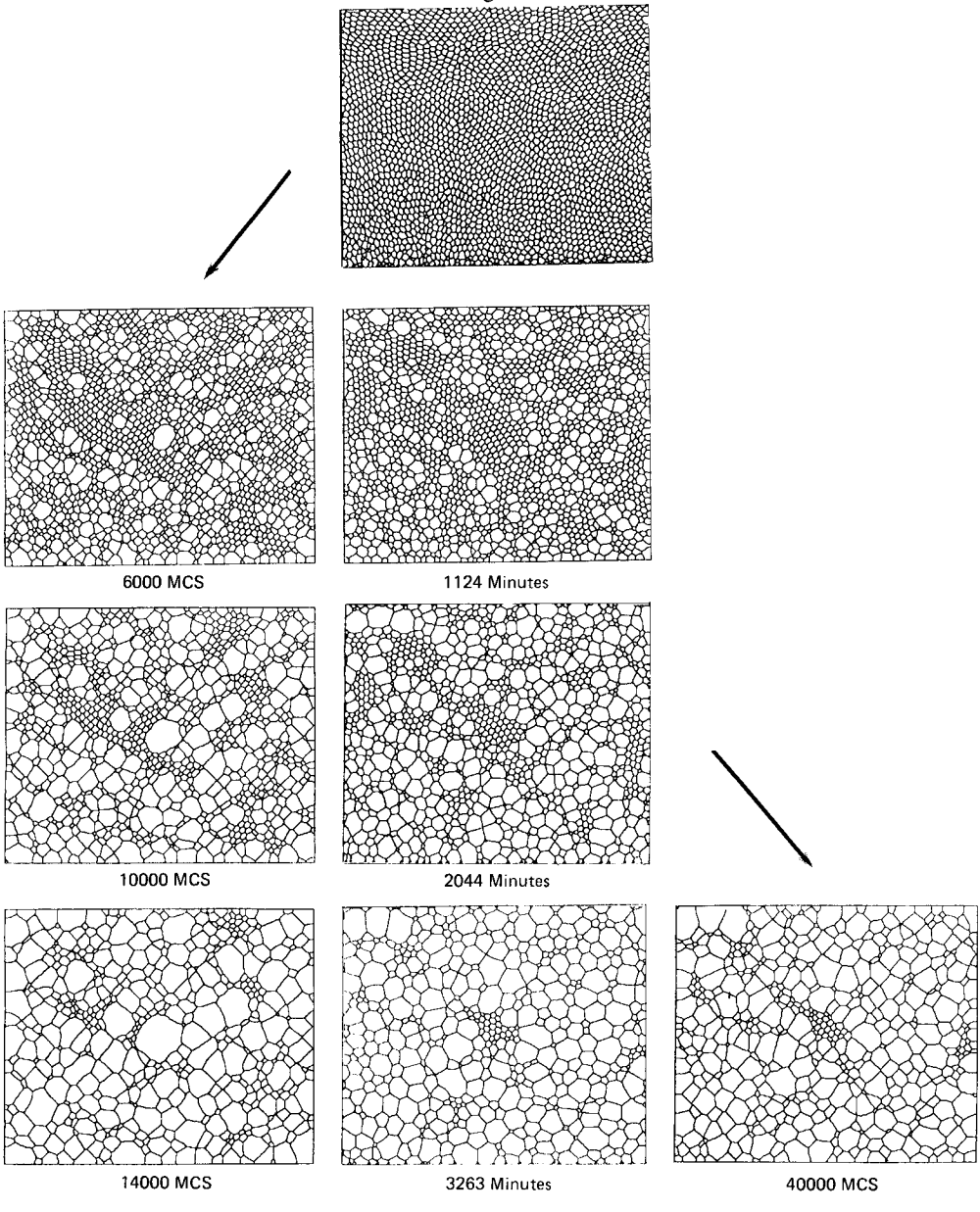

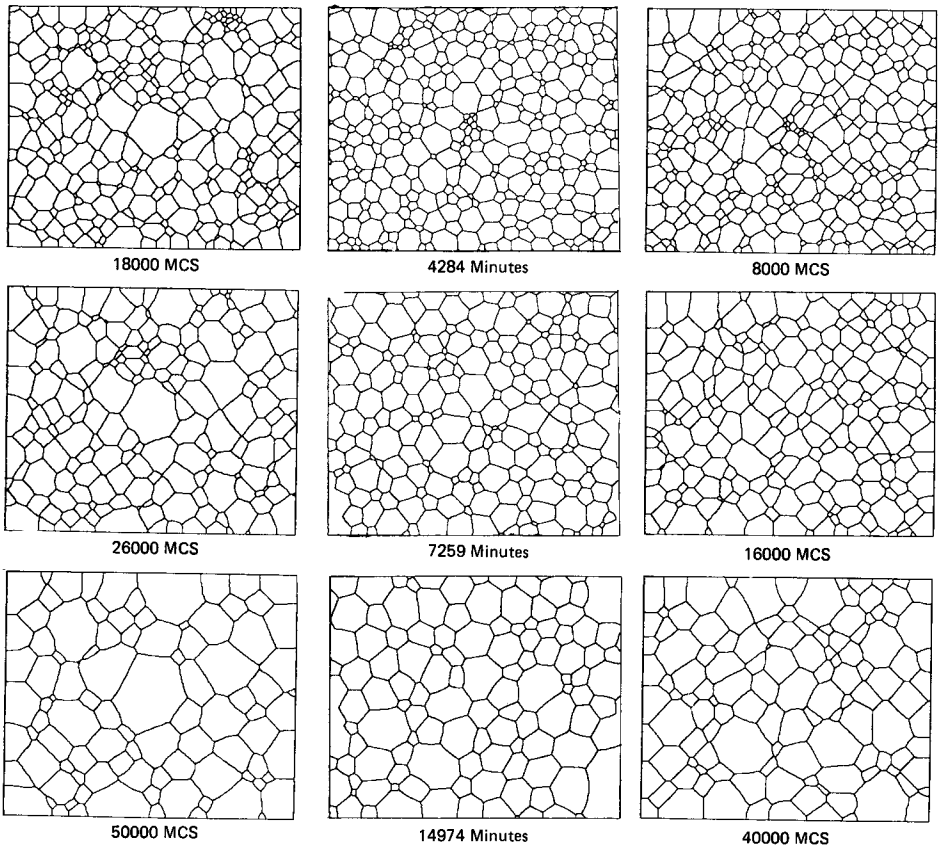

Potts model grain growth. Comparison of two-dimensional soap froth (centre) and the Potts model simulations on the square lattice starting with the digitized image at $t = 0$ min (left) and $t = 2044$ min (right): MCS, Monte Carlo steps. The areas shown are 30% details of the soap froth image and show the entire 600×500 pixel Potts model simulation.

deviating from the 120° rule (see fig. 2(*b*)). As a result, grain growth in a nearest-neighbour square-lattice Potts model tends to slow and finally to stop altogether as grain boundaries gradually align along preferred directions. In general, the effect of strong anisotropy is to produce exponents much less than unity. This effect is observed at low temperatures in many metals with a high anisotropy, which tend to have values of $\alpha \sim 0{\cdot}3$ (Beck 1954). One way to treat this problem in both model and experiment is to work at a higher temperature where fluctuations overcome anisotropy pinning. One finds experimentally in metals that higher temperatures result in larger growth exponents. However, the soap froth is essentially fluctuation-free and therefore should be simulated in the zero-temperature limit. The simulation method of Wejchert *et al.* (1986), avoids this problem by separating grain growth from pattern relaxation. Another solution is to use a nearest-neighbour hexagonal lattice (fig. 2(*a*); energy ratio, 1·15) or a next-nearest-neighbour square lattice (fig. 2(*c*); energy ratio, 1·13), to reduce pinning. There is still some preferred boundary alignment in both cases (e.g. along 45° and 90° orientations in the square lattice as seen in fig. 4) but $\alpha = 1$ and there is no evidence of freezing at least up to the length scale of the simulation. Srolovitz *et al.* (1983) have checked the anistropy effect in the hexagonal lattice by tracking the

evolution of an initially round grain. It becomes slightly hexagonal but continues to shrink essentially uniformly.

A second difficulty with the Potts model simulation is the range of length scales it requires. To measure successfully the scaling exponent for the growth of average grain area, for example, the following relation must hold:

$$L_{\text{lattice spacing}} \ll L_{\text{grain initial}} \ll L_{\text{grain final}} \ll L_{\text{lattice size}} \tag{3}$$

that is each grain must contain many spins, the grains must grow a substantial amount, and the final configuration must have many grains. This means that for truly reliable results the lattice needs to be at least 1000 spins per side. An insufficient appreciation of this problem led to some confusion over the actual scaling exponent of the model (Anderson *et al.* 1984, 1989, Frost, Thompson, Howe and Whang 1988).

We used two different types of Potts model for the simulations: a second-nearest-neighbour interaction on a square lattice to provide direct comparisons to the experiment, and a nearest-neighbour interaction on a triangular lattice to gather statistics on the scaling state. The simulations on a triangular lattice ran for $Q=48$, starting from a random initial state, on a 1000×1000 lattice with periodic boundary conditions. The run lasted 80 000 Monte Carlo steps. The square-lattice simulation ran on a 600×500 square lattice with open boundary conditions (in which spins on the boundary were assumed to interact with frozen imputities) starting from a digitized soap froth image. Here we used $Q=Q_{\max}$, where $Q_{\max}$ is the number of grains in the initial state. To compare results from the two simulations, we renormalized the time in the square-lattice simulation by $48/Q_{\max}$ so they are in the same relative units. Grain areas and topological distribution functions appear to be independent of the lattice type for simulations in which the boundaries do not freeze, but the two lattices in question have nearly identical anisotropies (Anderson *et al.* 1984) We are currently investigating the effect of lattice anisotropy on distributions. See Note added in Proof.

In the $Q=\infty$ Potts model, neither the motion of domain boundaries nor the disappearance of domains can lead to contact and hence coalescence of separate domains with the same spin type. Hence we explicitly exclude wall breakage from the simulation. Finite-Q Potts models allow grain coalescence and correspond to non-zero rates of wall breakage. In both cases, coalescence is a random process unrelated to the main mechanism of diffusive coarsening.

We ran square-lattice Potts model simulations using two different initial conditions, employing the digitized froth images at $t=0$ min ($Q_{\max}=2490$) and $t=2044$ min ($Q_{\max}=1175$) as the starting patterns. As seen in fig. 4, the $t=0$ min pattern is composed almost entirely of hexagonal bubbles of nearly equal area while the $t=2044$ min pattern has evolved sufficiently that there are few islands of six-sided bubbles remaining from the initial fill.

In fig. 4 we show the soap froth (30% detail) and the square-lattice Potts model simulation at various stages of evolution, beginning with identical initial patterns. The qualitative features of the disordering are similar, although the differing boundary conditions (the sample of the froth is taken from the bulk whereas the simulation has open boundary conditions) result in a rapid divergence between the actual patterns. A clear example of the difference in boundary conditions is the contact angle between the domain walls and the edges of the cell. In the experiment, the boundary of the viewing window does not affect the froth and the films can cross the boundary at an arbitrary angle. In the simulation (and adjacent to the actual cell walls in the experiment) the

angle of contact is always close to 90°. The digitization can also result in the appearance of spurious small bubbles near the image boundaries and occasional wall breakage that we attempt to correct for in our calculations. In the $t=2044$ min simulation, the disappearance of residual order occurs in both systems after the length scale has increased by approximately one order of magnitude and the qualitative patterns remain comparable. If we use the conversion that time is the number of Monte Carlo steps multiplied by 0·32, that is $t=t_m 0{\cdot}32$, which we discuss below, we find that, regardless of the initial random seed, the $t=0$ min simulation retains its hexagonal pattern for much longer than the froth. 'Crystal grains' composed of clusters of hexagonal bubbles seem more stable in the simulation than in the soap froth. Apparently six-sided bubbles are less likely to change their number of sides in the simulation than in a real froth. Once the blocks of hexagons disappear, however, and the length scale grows, the rate of evolution catches up and the long-term states of the $t=0$ min and $t=2044$ min simulations are indistinguishable. This difference indicates a fundamental although subtle difference in side redistribution between the simulation and real froth. Without further examination, however, it is difficult to say whether it is a true effect of an increased stability of hexagonal bubbles in the Potts model or, as suggested by the good agreement at larger length scales, results from the fact that the length scale of the initial pattern is small compared with the lattice constant.

In fig. 5 we compare the average bubble size as a function of time for the froth and simulations. Since the initial conditions of the simulations were taken from the same digitized images used to measure the areas of the bubbles in the froth, there was no freedom in assigning areas (which are measured in pixels) to bubbles. The multiplicative constant relating real time to Monte Carlo steps is a free parameter, however. We choose to fit the best match to the $t=2044$ min run and apply the conversion from Monte Carlo steps to minutes to the $t=0$ min run. The best fit for the former is $t(\text{min})=t_m 0{\cdot}32+2044$, where t_m is the number of Monte Carlo steps. In this case we have essentially exact agreement between the froth and the model up to 20 000 min where the statistics are best, after which both show fluctuations. The initial rate of area growth of the $t=0$ min simulation is significantly slower than that of the froth,

Fig. 5

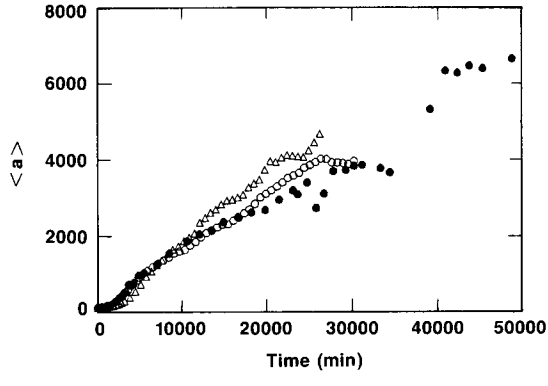

Area growth in soap froth. Average area (in pixels) against time for a two-dimensional air froth in a large cell: ●, experimental data for soap froth; ○, the Potts model simulations on the square lattice starting from the $t=2044$ min soap froth image; △,the Potts model simulations on the square lattice starting from the $t=0$ min soap froth image.

suggesting that the Potts model has more difficulty in converting order to disorder. In both cases, the typical qualitative dynamics for coarsening of an initially ordered froth appear: slow initial evolution, followed by rapid growth during which any residual order disappears, and a long-term tail with slower, approximately power-law growth (Glazier *et al.* 1987). We even obtain a purely fortuitous agreement in the long-time tails, where the soap froth and the $t = 2044$ min simulations both show non-monotonic changes in average area (at nearly the same time) owing to the contact with the cell boundary (and hence loss from the ensemble) of a large bubble. The growth exponent of both simulations appears to be slightly (though not significantly) higher than in the froth, a reminder that even the soap froth can exhibit non-ideal growth characteristics (Weaire and Bolton 1990). In all cases the exponent is compatible with a linear growth of average area in time ($\alpha = 1$).

§4. Distribution functions

Besides the mean bubble area, the two basic measures of the state of a froth are the distribution $\rho(n)$ of the number of sides, (the probability that a randomly selected bubble has n sides) and the normalized area distribution $\rho(a/\langle a\rangle)$ (the probability that a bubble has an area which is a given fraction of the mean bubble area).

A basic problem with any distribution function measured in a finite area is that large bubbles are more likely to touch the area's boundary (and hence to be excluded from the statistics) than are small bubbles. We therefore have a systematic bias against large (and many-sided) bubbles in our distribution functions and their moments. To the accuracies that we are able to measure, this error is not significant. For the second moment, the effective correction is of the order of 5%. It is relatively larger for higher moments. The mathematics of distribution function correction have been discussed in detail in Miles (1974), Lantuejoul (1978) and Blanc and Mocellin (1979).

We define the mth moment of the side distribution as

$$\mu_m \equiv \sum_{n=2}^{\infty} \rho(n)(n - \langle n\rangle)^m, \tag{4}$$

where $\langle n\rangle$ is the average number of sides of a bubble in the pattern (for infinite patterns $\langle n\rangle = 6$), and the absolute width of the distribution

$$W \equiv \sum_{n=2}^{\infty} \rho(n)|n - \langle n\rangle|. \tag{5}$$

For experimental distributions, $\langle n\rangle$ may differ from six; so our calculated values for the moments may differ slightly from those given elsewhere. The larger the difference between $\langle n\rangle$ and six, the less reliable is the distribution and the larger is the error in the moment estimate. Moments higher than μ_2 are sensitive to the large-n tail of the distribution, which is hard to measure, and thus are frequently only useful as qualitative indicators. W is useful because it is much less sensitive to small counting error fluctuations for large n than are the higher moments. We shall also refer to the ratio $R = \rho(5)/\rho(6)$—another simple reduction of the distribution.

While there are no general rules for correcting statistical errors, we find that small sample sizes tend to reduce average moments. For example, if there is a nominal 1% probability for 12-sided bubbles, the contribution to μ_2 should be 0·36. With a typical sample of 30 bubbles, however, we shall usually not see any 12-sided bubbles, and our estimate of μ_2 will be correspondingly low. The problem is worse for higher moments.

When possible, we attempt to correct for this bias by averaging several independent distributions. However, different distributions measured for the same time series are not truly independent, limiting our ability to compensate.

In fig. 6 we plot the evolution of the side distribution for the froth shown in fig. 4 which begins as a well ordered pattern with a side distribution sharply peaked at six. As a function of time the fraction $\rho(6)$ of six-sided bubbles decreases monotonically and the fraction $\rho(5)$ of five-sided bubbles increases monotonically. The large-n tail of the distribution first broadens and then narrows to an equilibrium width. At approximately 10 000 min (see fig. 4), just after the rate of evolution rolls over to a power law, the distribution becomes essentially time-independent, with $R = 1{\cdot}03$, confirming the existence of the scaling state noted by Stavans and Glazier (1989). We plot the scaling distribution for the triangular-lattice Potts model simulation and for the froth shown in fig. 3 in fig. 7. While $\rho(n)$ for the simulation lies within the range of measured values for each n, the froth distribution has fewer four- and many-sided bubbles.

In fig. 8 we plot μ_2 against time, which measures the r.m.s. width of the distribution, for the soap froth and, in fig. 9, for the $t = 0$ min square-lattice Potts model simulation. The large scatter results from the restricted size of the digitized image which limits the number of bubbles at long times. The last few points represent only about six bubbles each. Digitization errors also create some spurious many- and few-sided bubbles. We rechecked each distribution by hand, but some errors doubtless remained to contribute to the scatter. We observe the same basic pattern as that seen by Stavans and Glazier (1989). The initially narrow distribution composed mostly of hexagonal bubbles ($\mu_2 = 0$) widens to a maximum width $\mu_2 = 3{\cdot}25$ and then, at the same time that the rate of area growth rolls over into a power law ($t = 10\,000$ min; see fig. 5), narrows to a stable value of $\mu_2 = 1{\cdot}5 \pm 0{\cdot}3$, in agreement with the value $\mu_2 = 1{\cdot}5 \pm 0{\cdot}2$ measured by Stavans and Glazier (1989). In the simulation, μ_2 is qualitatively the same but increases slightly more slowly at short times and peaks slightly later and at a higher value of $\mu_2 = 4{\cdot}4$. It

Fig. 6

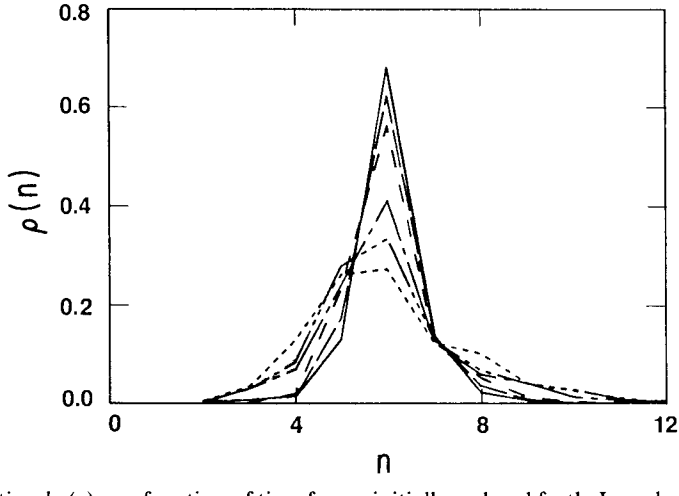

Side distribution l $\rho(n)$ as a function of time for an initially ordered froth. In order of decreasing $\rho(6)$, measurement times were $t = 0$ min, $t = 545$ min, $t = 1124$ min, $t = 1565$ min, $t = 2044$ min and $t = 3163$ min. Note that the distribution first broadens and then narrows to its equilibrium shape.

Fig. 7

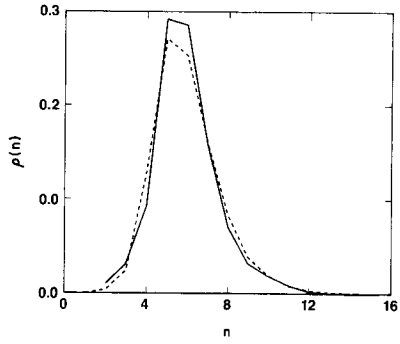

Scaling-state side distributions for the soap froth (——) and for the triangular-lattice Potts model simulation (– – –).

Fig. 8

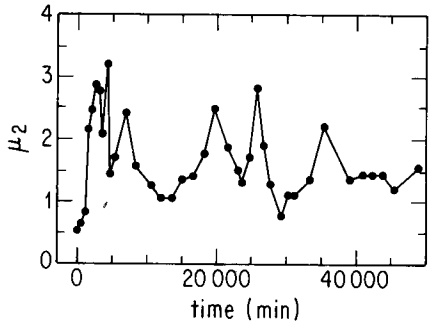

Second moment μ_2 of the side distribution as a function of time for the soap froth.

Fig. 9

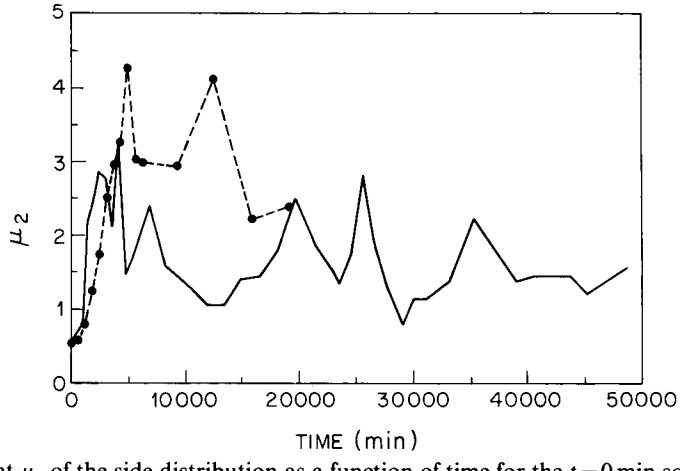

Second moment μ_2 of the side distribution as a function of time for the $t=0$ min square-lattice Potts model simulation (– – ● – –). The soap froth values are reproduced for reference (——).

Fig. 10

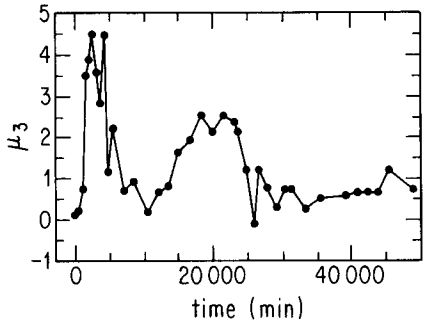

Third moment μ_3 of the side distribution as a function of time for the soap froth.

Fig. 11

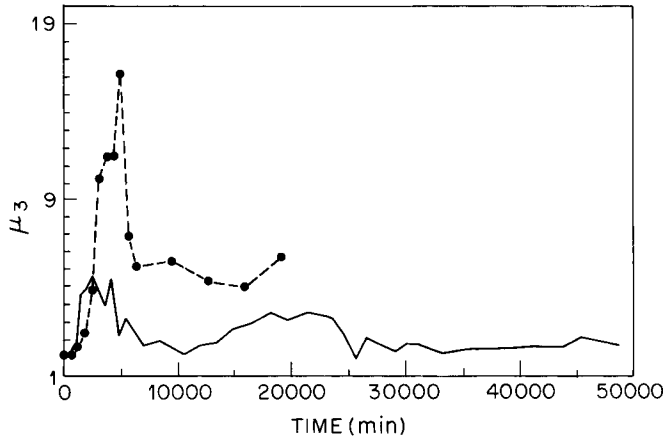

Third moment μ_3 of the side distribution as a function of time for the Potts model simulation (-- ● --) on the square lattice starting from the $t=0$ min digitized soap froth image. The soap froth values are reproduced for reference (——).

then decreases to an equilibrium value of roughly $2{\cdot}4 \pm 0{\cdot}1$ in agreement with the $t=2044$ min simulation and somewhat larger than the soap froth.

The higher moments follow the same pattern. We have calculated the evolution of μ_3 for the soap froth (fig. 10) and the $t=0$ min square-lattice Potts model simulation (fig. 11), μ_4 for the soap froth (fig. 12) and simulation (fig. 13), and W for the froth (fig. 14) and the simulation (fig. 15). In the froth, the third moment, which measures the asymmetry of the distribution, in this case mostly the strength of the large-n tail, begins near zero, increases rapidly to a maximum during equilibration when the frequency of many-sided bubbles is maximal ($\mu_3 = 4{\cdot}5$) and then drops to a stable value of $\mu_3 = 1{\cdot}0 \pm 0{\cdot}5$. The graph suggests that μ_3 may undergo a second oscillation, undershooting the stable value at around 10000 min and reaching a second slightly lower maximum of $\mu_3 = 2{\cdot}5$ at around 20000 min. If so, it is a surprising confirmation of the prediction by Beenakker (1986) that equilibration should require multiple oscillations because cohorts of bubbles in an initially ordered pattern shrink and disappear in phase. The simulation shows the same large peak, slightly delayed, with a hint of a second peak at

Fig. 12

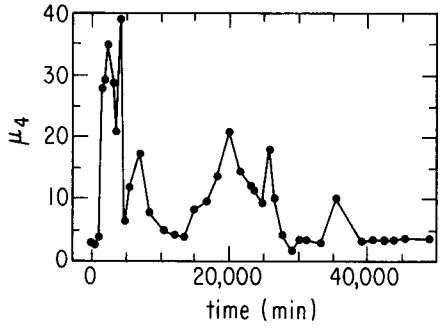

Fourth moment μ_4 of the side distribution as a function of time for the soap froth.

Fig. 13

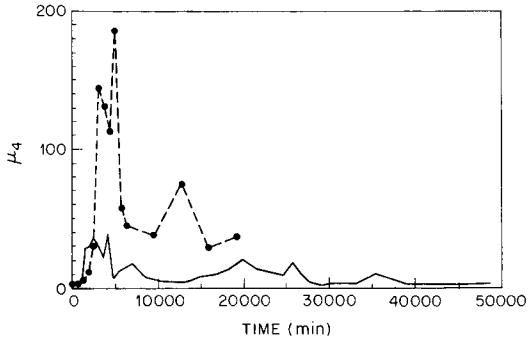

Fourth moment μ_4 of the side distribution as a function of time for the Potts model simulation (-- ● --) on the square lattice starting from the $t = 0$ min digitized soap froth image. The soap froth values are reproduced for reference (——).

Fig. 14

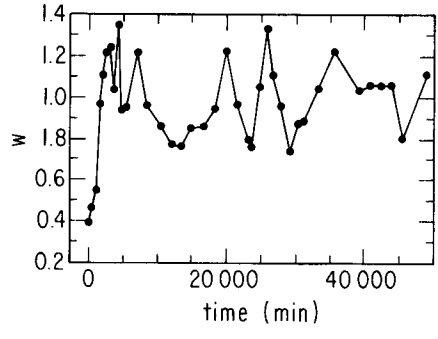

Absolute width W of the side distribution as a function of time for the soap froth.

Fig. 15

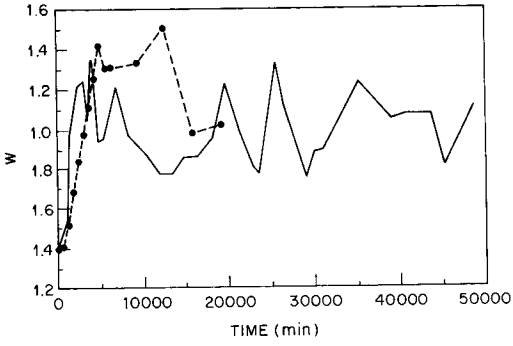

Absolute width W of the side distribution against time for the Potts model simulation (– – ● – –) on the square lattice starting from the $t = 0$ min digitized soap froth image. The soap froth values are reproduced for reference (——).

the end of the data at $t = 20\,000$ min. The notch seen in the froth at $t = 4000$ min finds a weak echo in the simulation. As befits a measure sensitive to the large-n tail, the peak value of $\mu_3 = 16{\cdot}6$ and the scaling state value of $\mu_3 = 5{\cdot}25 \pm 1{\cdot}25$ are larger than in the soap froth.

Nothing changes if we look at the fourth moment which represents the flatness of the distribution, essentially the relative strength of $\rho(4)$, $\rho(7)$ and $\rho(8)$ against $\rho(5)$ and $\rho(6)$. In the froth, the initial value is $\mu_4 = 5$. It then grows to $\mu_4 = 40$ and decreases, with a possible oscillation and second peak at 20 000 min, to a stable value of $\mu_4 = 6{\cdot}0 \pm 3{\cdot}5$. The simulation shows the expected delay and increased values with a maximum of $\mu_4 = 185$ and a scaling-state value of $\mu_4 = 35 \pm 10$, with a suggestion of a second oscillation at around $t = 14\,000$ min. The agreement in the notches in the main peaks of the froth and simulation is more pronounced, suggesting that it results from side shedding in a single very-many-sided bubble.

We call the initial maximum in all distribution functions, the *equilibrating maximum*. We might speculate that the second maximum that we observe in the third and fourth moments represents the decay of next-nearest-neighbour correlations while the first peak represents the decay of nearest-neighbour correlations. In that case the time between the peaks would represent the time for an average bubble to disappear, and hence for disorder to propagate a distance of one bubble radius. The oscillation might also result from a phase lag caused by different time constants for area and side equilibration. However, without values for μ_3 and μ_4 from additional experimental runs, we assume that the apparent oscillation is a statistical artefact, which could result if, for example, a single very-many-sided bubble appeared at roughly 15 000 min and gradually began to shed sides after 20 000 min. We mention this scenario as an example only, since we saw no single many-sided bubble in the experiment to throw off our calculations.

In the froth the absolute width increases from an initial minimum of $W = 0{\cdot}4$ to a stable value ($W = 1{\cdot}1 \pm 0{\cdot}3$) at around 10 000 min, with a possible weak maximum of $W = 1{\cdot}3$ at 5000 min. Any oscillation at 20 000 min is lost in noise. The simulation shows delay but little overshoot, with a maximum of $W = 1{\cdot}5$ and a scaling value of $W = 1{\cdot}0 \pm 0{\cdot}1$. The agreement between the two low moments and the disagreement for the higher moments implies that the simulation creates a few more very-many-sided

Table 1. Side distribution functions.

Reference	System	$\rho(3)$ ($\rho(10)$)	$\rho(4)$ ($\rho(11)$)	$\rho(5)$ ($\rho(12)$)	$\rho(6)$ ($\rho(13)$)	$\rho(7)$ ($\rho(14)$)	$\rho(8)$ ($\rho(15)$)	$\rho(9)$ ($\rho(2)$)
					Experiment			
Glazier (1989)	Two-dimensional froth soap	0·010 (0·008)	0·091 (0·005)	0·314 (0·0008)	0·305 (0·0003)	0·170	0·069	0·033
	Error, ±	0·013 (0·008)	0·011 (0·007)	0·023 (0·001)	0·017 (0·0007)	0·027	0·006	0·013
Fradkov *et al.* (1985b)	Metal grains, Al 10^{-4} Mg 0·22 mm foil	0·035 (0·020)	0·140 (0·009)	0·259 (0·002)	0·246 (0·0025)	0·157 (0·0012)	0·082 (0·0013)	0·036 (0·0016)
	Error, ±	0·002 (0·005)	0·007 (0·003)	0·016 (0·003)	0·019 (0·003)	0·009 (0·002)	0·005 (0·002)	0·006 (0·002)
					Theory			
Crain (1978)	Voronoi model, $N = 57\,000$	0·0110 (0·0075)	0·1078 (0·0014)	0·2594 (0·00018)	0·2952 (0·00005)	0·1984	0·0896	0·0296
Kikuchi (1956)	Maximum-entropy model I	0·035 (0·015)	0·141 (0·001)	0·233	0·238	0·185	0·107	0·045
Soares *et al.* (1985)	Vertex model, straight sides	0·027 (0·009)	0·149	0·229	0·223	0·198	0·125	0·040
Kawasaki *et al.* (1989)	Vertex model II	0·031 (0·019)	0·141 (0·006)	0·253 (0·002)	0·237	0·173	0·094	0·045
Marder (1987)	Mean-field theory	0·011 (0·015)	0·076 (0·008)	0·263 (0·006)	0·414	0·123	0·056	0·029
Blanc and Mocellin (1979)	Mean-field theory	— (0·021)	0·190 (0·006)	0·259 (0·0009)	0·230	0·160	0·094	0·050
Fradkov *et al.* (1985a)	Network model	0·018 (0·010)	0·115 (0·003)	0·262	0·273	0·184	0·089	0·033
	Potts model, triangular lattice	0·025 (0·019)	0·128 (0·008)	0·271 (0·003)	0·253	0·161	0·084	0·039

Table 2. Side distribution moments.

System	Reference	$\langle n \rangle$	μ_2	μ_3	μ_4	W
				Experiment		
Two-dimensional soap froth	Glazier (1989)	5·933	1·486	1·105	7·154	0·940
Metal grains, Al + 10^{-4} Mg foil	Fradkov *et al.* (1985 b)	5·952	2·900	5·013	43·90	1·269
				Theory		
Voronoi model, $N = 57\,000$	Crain (1978)	5·997	1·777	1·026	10·68	1·013
Maximum-entropy model I	Kikuchi (1956)	5·982	2·399	1·208	15·51	1·223
Vertex model	Soares *et al.* (1985)	5·997	2·273	0·740	12·63	1·213
Vertex model II	Kawasaki *et al.* (1989)	5·979	2·544	2·288	20·75	1·239
Mean-field theory	Marder (1987)	6·005	1·909	3·287	21·57	0·905
Mean-field theory	Blanc and Mocellin (1979)	5·976	2·489	2·881	19·18	1·244
Network model	Fradkov *et al.* (1985a)	5·554	2·758	0·983	20·36	1·358
Potts model		5·978	2·490	2·971	23·22	1·196

bubbles than the real froth does. These extra bubbles suggest that side shedding is more strongly anticorrelated in the froth than in the simulation.

In table 1, we give side distributions for the soap froth, metallic grain growth in aluminium films, and a few of the better known coarsening simulations. We give corresponding moments in table 2. We note that in this table the moments are exactly as calculated from the published distributions (Glazier 1989).

In spite of the large error bars in our distribution measurement, the scaling-state side distribution of the soap froth is surprisingly difficult to match theoretically. The Voronoi construction is out of range as is the maximum-entropy model of Kikuchi. Of the topological mean-field theories, Marder's (1987) model gives an excessively high value of μ_3 because of its correlated side redistribution which tends to make many-sided bubbles gain sides and thus stretch the large-n tail. The model of Blanc and Mocellin (1979) for two-dimensional growth (no nucleation of three-sided bubbles) with no side-shedding correlations is also tail heavy. The network model of Fradkov *et al.* (1987) has difficulty matching both μ_2 and μ_3 for a given rate of side swapping but does a reasonable qualitative job. The vertex model of Kawasaki *et al.* (1989) does reasonably well with the moments but has far too many four-sided bubbles. The boundary dynamics model of Soares, Ferro and Fortes (1985) is also tail heavy. Unfortunately we lack scaling-state data for the two models that seem most promising on physical grounds: the boundary dynamics model of Frost and Thompson (1987) and the modified Potts model of Wejchert *et al.* (1986). The Potts model simulations' moments are high, as we expect from the stretched tail.

If we try to match the froth to other experimental coarsening patterns, the only experiment that provides a reasonable match is the measurement of two-dimensional grain growth in $Al+10^{-4}Mg$ foil by Fradkov *et al.* (1985b, 1987). The side distributions are similar in shape with $R=1{\cdot}05$ for the grain growth and $R=1{\cdot}03$ for the froth. The chief difference is the prominence of the tail in the metallic grain growth. Nevertheless, because of the large scatter in both measurements, the measured range of distributions and moments overlap in all categories. Unsurprisingly, the network model of Fradkov *et al.* with the rate of T1 processes set to be about five times the rate of T2 processes agrees well with their experimental data for the foil. The Potts model also is within range of the results for the foil for all values, although consistently on the low side for the moments.

The apparent failure of topological mean-field theories and network models to predict the moments in the soap froth correctly is surprising—but given the large uncertainties in the experimental distributions hardly conclusive. There seems to be an anti-many-sided bubble bias built into the soap froth. Any successful mean-field theory needs to include an anticorrelation in side shedding; that many-sided bubbles preferentially lose sides and few-sided bubbles preferentially gain sides. A possible source for this anticorrelation is the deviation of internal angles from the predicted 120°. Marder's model, which assumes a positive correlation, gives a clearly worse result than assuming uncorrelated redistribution.

In the case of the Potts model and metallic grain growth the discrepancy may arise from stiffness caused by lattice anisotropy. The excess curvature which opposes increases in number of sides for many-sided bubbles is masked in the presence of anisotropy. In this case we would expect that the third moment would increase with increasing anisotropy. Unfortunately we have no data on the dependence of the distribution functions on the relative orientational anisotropies of the Potts model and metal films. (See Note added in proof.) For lower anisotropies and higher temperatures,

the frequency of many-sided bubbles should decrease. An additional factor may come from the relative rates of diffusion along and across grain boundaries. We expect that the Potts model and metal grains will be further from equilibrium than a soap froth and hence may eliminate many-sided bubbles more slowly, since a bubble may not 'know' how many sides it really has. Again, careful measurements using different materials and temperatures are needed. That the metal film gives a larger tail than the Potts model suggests that anisotropy and not equilibration effects predominate, but this conclusion is far from certain.

We tentatively assert the existence of a universal distribution function for two-dimensional coarsening including the soap froth, two-dimensional grain growth in metals and the Potts model. It seems that the soap froth has a lower frequency of many-sided bubbles than Potts model has, and that the Potts model has a lower frequency of many-sided bubbles than real grain growth has. However, with our current data, we cannot always distinguish individual examples of distributions belonging to the three cases. In particular we have no way to determine whether a larger or smaller frequency of many-sided bubbles is 'ideal'. We cannot tell whether disequilibria or anisotropies in the Potts model cause a deviation from the ideal coarsening of the soap froth, or whether an anti-many-sided bubble bias due perhaps to deviations from 120° angles causes the soap froth to deviate from the ideal coarsening of the Potts model. It seems probable, however, that the soap froth comes closest to ideal behaviour. We certainly need better experimental data, especially a scaling state for the soap froth with many (i.e. thousands of) bubbles.

If we examine the time evolution of the area histograms (fig. 16) for the two-dimensional soap froth, $\rho(a/\langle a\rangle)$, we find roughly the same scenario that we found for side distributions. At short times the distribution peaks sharply around the average area (corresponding to a pattern composed primarily of uniform-sized six-sided bubbles). As time passes, the most probable size gradually decreases to zero while the large-area tail of the distribution gradually lengthens. This broadening comes about because the fraction of shrinking small bubbles with near-zero absolute area remains essentially constant, while the relative size of small bubbles decreases as the total length scale increases. Eventually the distribution reaches a time-invariant scaling state (fig. 17). The number of small nearly-average-area bubbles is greater in the simulation than

Fig. 16

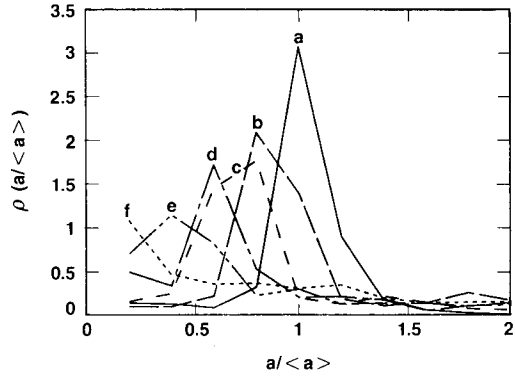

Evolution of the area distribution as a function of time for an initially ordered froth. The times are as follows: (*a*) $t=0$ min; (*b*) $t=545$ min; (*c*) $t=1124$ min; (*d*) $t=1565$ min; (*e*) $t=2044$ min; and (*f*) $t=3163$ min.

Fig. 17

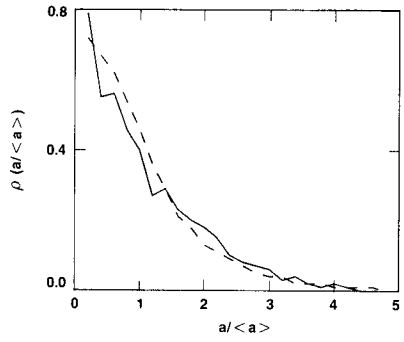

Scaling-state normalized area distribution for the soap froth (——) and the triangular-lattice Potts model simulation (– – –).

Fig. 18

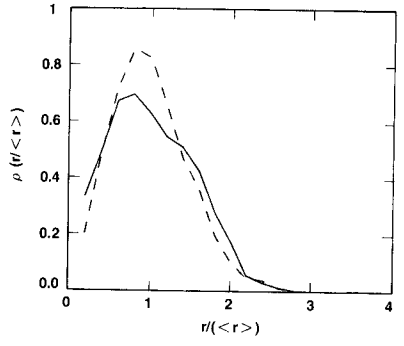

Scaling-state normalized radius distribution for soap froth (——) and the triangular-lattice Potts model simulation (– – –).

in the soap froth (i.e. the distribution is narrower), but the distributions are otherwise very close. We see the differences more clearly if we plot $\rho(r/\langle r\rangle)$ (fig. 18). In this distribution the simulation shows a strong peak around the average radius, while the froth has a less pronounced peak and broader tail. Since the widths of the area and side distributions increase and decrease together during the initial period of disordering, it seems somewhat paradoxical that in the scaling state the simulation should have a wider side distribution and narrower area distribution than the froth.

We next examine the scaling-state distributions more closely. In fig. 19 we plot area distributions for five-, six-, seven- and eight-sided bubbles for the froth and for the triangular-lattice Potts model simulation. As we might expect for bubbles which shrink, the most probable area for a five-sided bubble is zero, agreeing with the simulation. Six-sided bubbles have a relatively narrow width around the average area, with good agreement between the experiment and the simulation. Both seven- and eight-sided bubbles are larger, with broader distributions than the six-sided bubbles. The simulation seems to give a higher third moment than the actual froth for these types (again we may suppose that this is an anisotropy effect), but the difference is statistically significant only for seven-sided bubbles.

Fig. 19

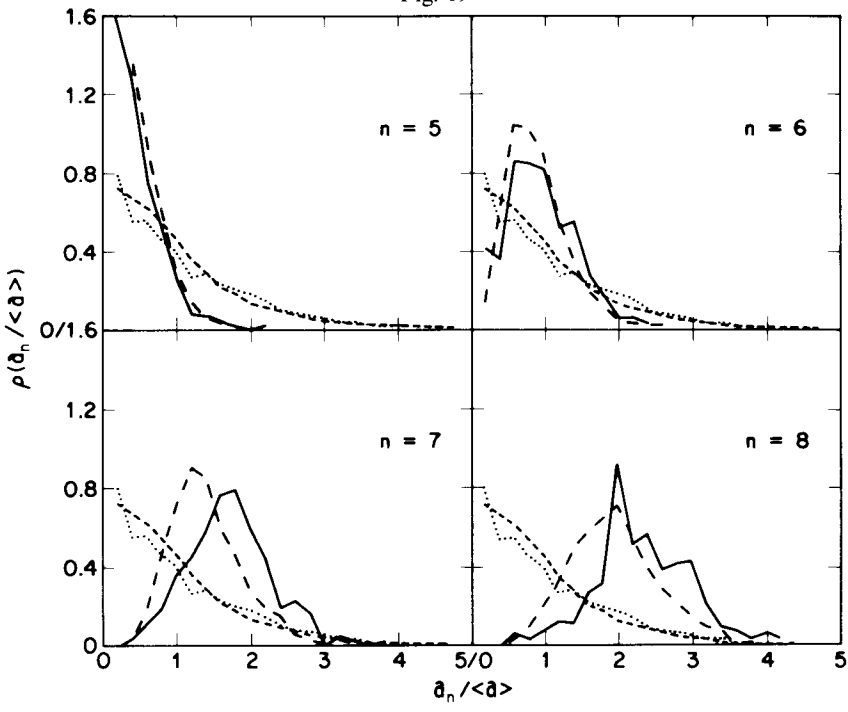

Correlated area distributions for five-, six-, seven- and eight-sided bubbles in the scaling state. Measurements are for the soap froth (——) and the triangular-lattice Potts model simulation (— —). Total area distributions are shown for reference for the soap froth (·····) and the triangular-lattice Potts model simulation (– – –).

§5. 'Lewis' law'

Of the aggregate quantities derivable from the area distribution functions, the average area of an n-sided bubble as a function of n is the most robust diagnostic. The most commonly assumed relation is that of Lewis (1928), originally proposed for the epithelial cells of the cucumber, that the area of a polygonal cell should be a linear function of its number of sides, that is

$$\langle a_n\rangle = c_1 + c_2 n \tag{6}$$

at any fixed time, where c_1 and c_2 are fitting parameters.

We present experimental measurements of normalized bubble area (i.e. $\lambda_n = \langle a_n\rangle/\langle a\rangle$) as a function of n in fig. 20 along with the results of the square- and triangular-lattice Potts model simulations. To our numerical uncertainty the three results are indistinguishable. We observe that the area for few-sided ($n = 3, 4$) bubbles is larger than that predicted by Lewis' law. Indeed, for many runs, a linear fit actually predicts negative areas for three- and four-sided bubbles. Many-sided ($n > 8$) bubbles are smaller than predicted as well, although this discrepancy may be due to memory of the initial length scale.

In table 3 we present side–area correlations for a few models and experimental systems. We normalize $\langle a_6\rangle$ to unity, which is not ideal (we would prefer to look at λ_n) but is at least consistent and does not require us to know $\langle a\rangle$ for all categories. We can easily distinguish the biological patterns which obey Lewis' law from the coarsening patterns which do not. The correlations for the soap froth and two-dimensional grain

Fig. 20

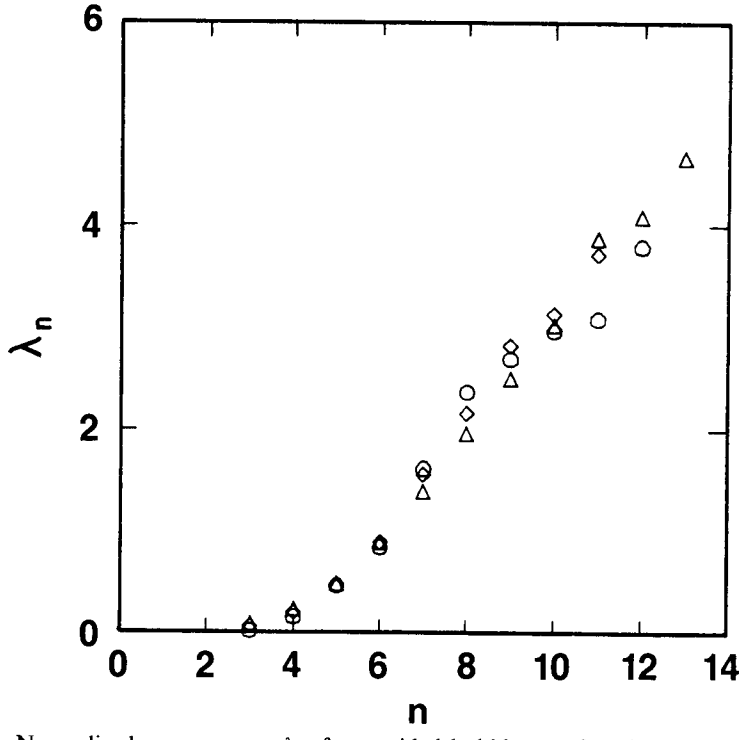

Lewis' law. Normalized average area λ_n of an n-sided bubble as a function of n for the two-dimensional soap froth (○) and the Potts model simulation on a triangular lattice (△) and a square lattice (◇). To within experimental error the correlations are identical.

growth in aluminium are comparable for large n. For small n, the aluminium grains are much larger than bubbles, suggesting a mechanism stabilizing small few-sided grains in the metal. As noted, the Potts models give almost identical results to the froth. The vertex model of Nakashima *et al.* (1989) also does well. The mean-field theories all tend to have both few- and many-sided bubbles too large, again suggesting a failure to consider an anticorrelation in side redistribution. In the froth, large few-sided bubbles are less likely to lose sides than small few-sided and large many-sided bubbles, and thus there are fewer large few-sided bubbles produced than predicted by the uncorrelated mean-field theories. As we might expect the Voronoi construction is out of range, as are the maximum-entropy models.

If we plot instead $r_n = \langle a_n^{1/2} \rangle / \langle a^{1/2} \rangle$, originally discussed in the context of three-dimensional grain growth (Feltham 1957) (fig. 21), the graph is significantly more linear, with just a hint of S-curve roll-over for large n. In this case because of the scarcity of many-sided bubbles we may well be observing the selection effect previously discussed; large many-sided bubbles are more likely to intersect the frame boundary than are small bubbles and are hence more likely to be excluded from consideration, resulting in a low apparent size for large n. Once again we find that the soap froth, and the square- and triangular-lattice Potts model simulations give essentially identical results. We summarize the available data for other models in table 4. Once again we have used the normalization $r_6 = 1$. The agreement between the soap froth and the aluminium foil is reasonable, although the foil has slightly larger many-sided grains. As we would expect,

Table 3. Lewis' law, for more complete tables see Glazier (1989).

System	Reference	A_3 (A_2)	A_4	A_5	A_6 (A_{11})	A_7 (A_{13})	A_8 (A_{13})	A_9 (A_{14})	A_{10}
					Experiment				
Soap froth		0·04	0·18	0·56	1·00 (4·61)	1·96	2·84	3·19	3·75
Al + 10^{-4} Mg 0·22 mm foil	Fradkov *et al.* (1985b)	0·12 (0·16)	0·37	0·56	1·00 (4·35)	1·41 (5·15)	2·12	3·25	3·55
Cucumber 100 mm	Lewis (1928)	—	0·51	0·76	1·00	1·29	1·49	1·60	
					Theory				
Mean-field theory	Marder (1987)	0·24	0·35	0·56	1·00 (3·18)	1·53 (3·60)	2·04	2·49	2·93
Network model	Fradkov *et al.* (1985a)	0·53	0·53	0·71	1·00 (6·47)	1·96 (7·71)	2·80	3·95	4·91
Network model	Beenakker (1988)	0·38	0·46	0·62	1·00 (5·35)	1·75	2·63	3·49	4·39
Voronoi model	Crain (1978)	0·51	0·66	0·82	1·00	1·17	1·35	1·55	1·67
Potts model		0·03	0·23	0·53	1·00 (4·37)	1·83 (4·70)	2·35 (—)	3·07 (5·37)	3·53
Vertex model II	Nakashima *et al.* (1989)	0·002	0·17	0·45	1·00 (4·36)	1·72 (5·13)	2·39	3·06	3·64

Fig. 21

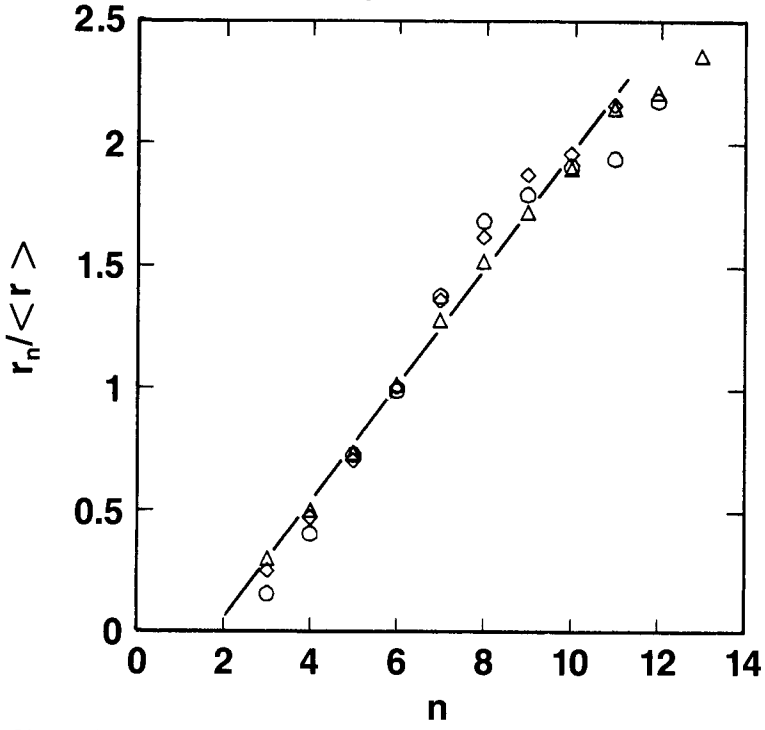

Radius law. Normalized average radius of an n-sided bubble for the two-dimensional soap froth (○) and the Potts model simulation on a triangular lattice (△) and a square lattice (◇). To within experimental error the correlations are identical.

the Potts model and the vertex model of Kawasaki *et al.* (1989), Nakashima *et al.* (1989) and Enomoto *et al.* (1989) give the best agreement with experiment. The uncorrelated mean-field theories predict excessively large few-sided bubbles. In all cases the overall linearity of the correlation is good, and the radius law

$$\langle r_n \rangle = c_1 + c_2 n \tag{7}$$

seems verified for both two- and three-dimensional grain growth, at least for n small enough that we are able to obtain reasonable statistics.

Our conclusion is twofold. The radius law works for grain growth while Lewis' law fails (although the latter works for biological aggregates with constrained area distributions). Also, all the models that seem physically reasonable give good agreement with experiment, the models that we think of as coming closest to the actual physics, such as the Potts model, giving the best results. The agreement also provides added evidence for the existence of an anticorrelation in side redistribution, which is apparent in the mean-field theory's predictions of a larger size for few-sided bubbles.

§6. The Aboav–Weaire law

The simplest side correlation function to measure (and the only one that can be reliably calculated given the available statistics) is the average number $m(n)$ of sides of the neighbours of an n-sided bubble (Aboav 1970). Several authors have assumed statistical equilibrium and short-range interactions to calculate the form of this function (Weaire 1974, Rivier 1985, Lambert and Weaire 1981, 1983).

Table 4. Radius law.

System	Reference	r_3	r_4	r_5	r_6 (r_{11})	r_7 (r_{12})	r_8 (r_{13})	r_9 (r_{14})	r_{10}
					Experiment				
Soap froth		0·15	0·40	0·73	1·00 (1·96)	1·40 (2·21)	1·71	1·82	1·93
Al + 10^{-4} Mg 0·22 mm foil	Fradkov *et al.* (1985b)	—	0·48	0·72	1·00 (2·23)	1·13 (2·52)	1·58 (—)	1·93 (2·76)	2·10
					Theory				
Topological	Fradkov *et al.* (1985a)	0·57	0·61	0·76	1·00 (2·21)	1·38	1·67	1·96	2·13
Vertex model II	Nakashima *et al.* (1989)	0·15	0·36	0·64	1·00 (2·40)	1·56	1·76	1·93	2·15
Vertex model	Enomoto *et al.* (1989)	0·16	0·27	0·64	1·00	1·34	1·59	1·66	
Topological	Beenaker (1988)	0·62	0·66	0·77	1·00	1·37	1·70	1·99	2·23
Potts model		0·27	0·49	0·73	1·00 (2·17)	1·34 (2·22)	1·60 (2·39)	1·82	1·95

We may argue as follows. Assume that there are no long-range correlations or stresses in the lattice. Then *topological charge* ($\tau \equiv n-6$, which represents the residual stress around an n-sided bubble) should be locally screened. Consider an n-sided bubble. Its topological charge is $\tau = n-6$. Therefore, nearest-neighbour charge screening requires that the bubble's nearest neighbours must have a total topological charge of $\tau = 6-n$. Thus the average topological charge of each neighbour is $\tau = (6-n)/n$; so

$$m(n) = 6-(6-n)/6 = 5+6/n. \tag{8}$$

A longer-range interaction with weak local correlation will change the constants, but we expect a general form

$$m(n) = \kappa_1 + c/n. \tag{9}$$

Weaire has argued on physical grounds that the correct form of the relation is

$$m(n) = 6-a+(6a+\mu_2)/n, \tag{10}$$

where μ_2 is the second moment of the side distribution and a is a constant of order one (Lambert and Weaire 1981, 1983). This relation is known as the Aboav–Weaire law.

In fig. 22 we present experimental $m(n)$ for the soap froth and the square- and triangular-lattice Potts model simulations. The results are essentially identical with no free parameters. We can extend the comparison by plotting $\rho_m(n)$, the probability that a bubble next to an m-sided bubble has n sides. We present results in fig. 23 for the soap

Fig. 22

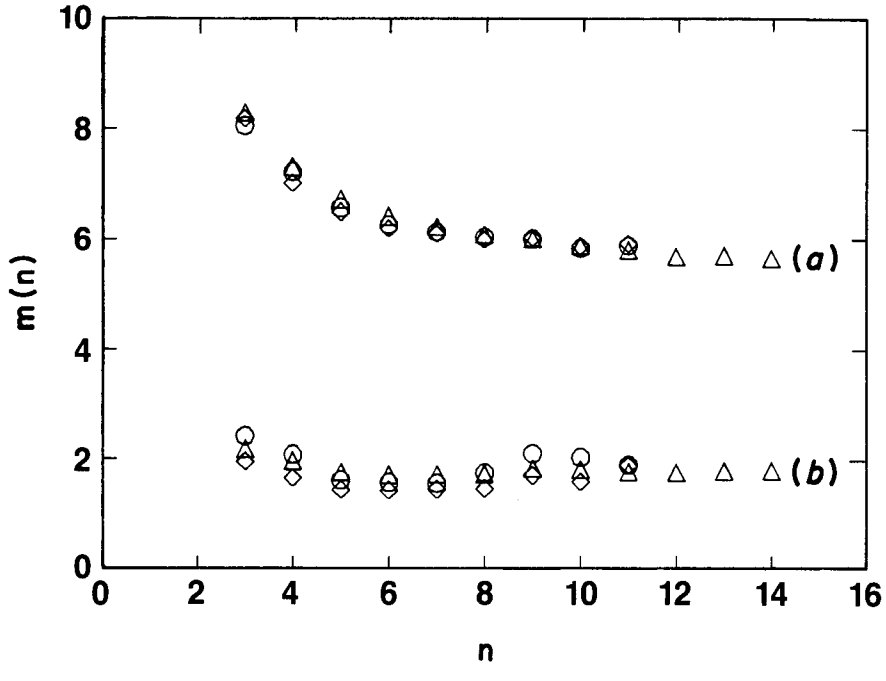

Correlation between the number of sides of neighbouring bubbles. $m(n)$ is the average number of sides of a bubble next to an n-sided bubble. (*a*) The value of $m(n)$ and (*b*) the standard deviation for the soap froth (○) and the Potts model simulations on a triangular lattice (△) and a square lattice (◇). To within experimental error the correlations are identical.

Fig. 23

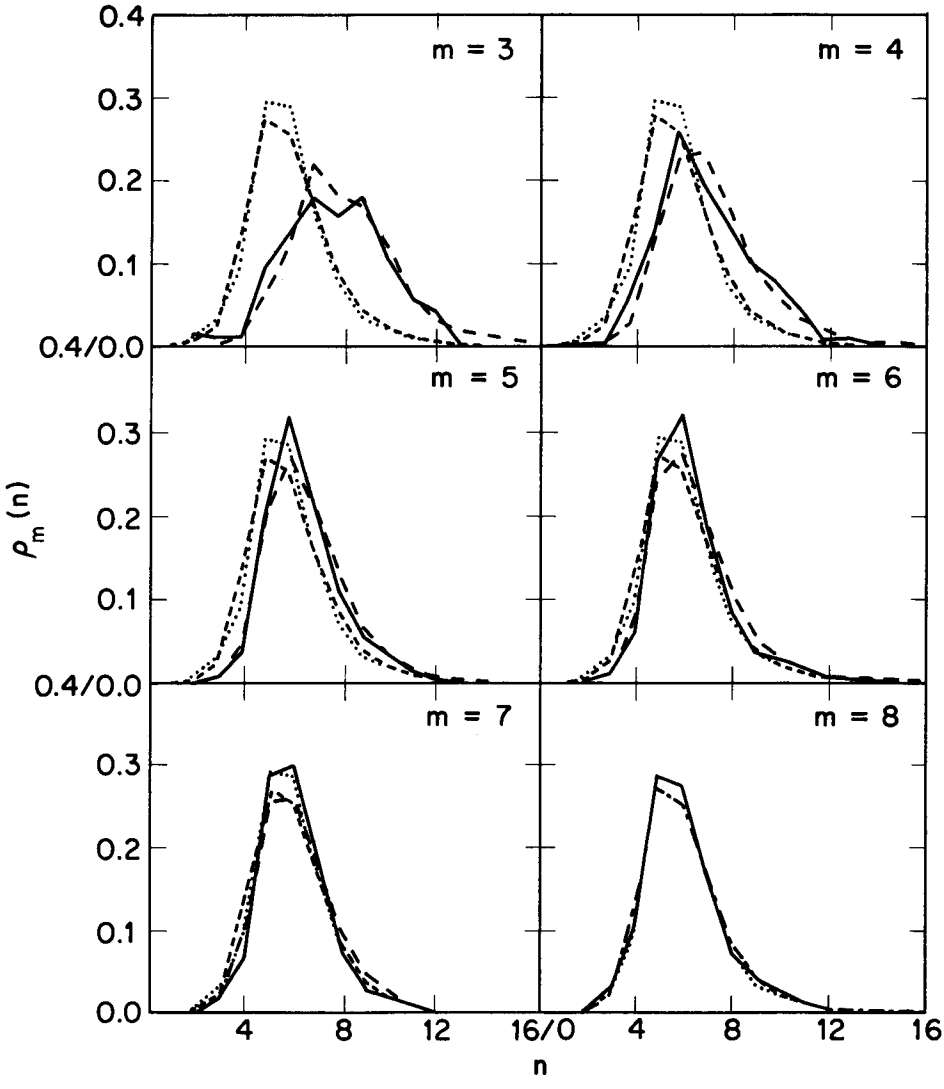

Correlated side distributions of bubbles next to m-sided bubbles in the scaling state: (——), distribution for the froth; (— —), and the triangular-lattice Potts model simulation. The total distribution function $\rho(n)$ is given for reference for the soap froth (· · · · ·) and for the triangular-lattice Potts model simulation (– – –).

froth and the triangular-lattice Potts model simulation. As expected, we find that few-sided bubbles tend to be near many-sided bubbles. The converse does not hold, however. Six-sided bubbles like to cluster together, and seven-sided bubbles attract six-sided bubbles. Even more surprising, the distribution of neighbours of eight-sided bubbles is essentially the total distribution. Discounting the bias towards many- and few-sided bubbles that we have noted in the simulation, the behaviours of the distributions as a function of m are identical for the simulation and the froth.

§7. Other measures of disorder

We have previously discussed several distribution function measures of the equilibration and disordering of a cellular pattern (Glazier *et al.* 1987, Glazier 1989, Stavans and Glazier 1989). Another natural way to look at disorder is to calculate an entropy. However, calculating the entropy of a pattern directly is sensitive to low-amplitude noise and to lattice discretization. We therefore follow a suggestion made by J. Gollub (1989, private communication) for the analysis of the pattern of convective rolls in a large-aspect-ratio Rayleigh–Bénard cell and measure the entropy of the azimuthally averaged two-dimensional Fourier transform of the pattern:

$$\left.\begin{aligned} f_0(k) &= \int f(x)\exp(\mathrm{i}\mathbf{x}\cdot\mathbf{k})\,\mathrm{d}x, \\ f(k) &= f_0(k)\Big/\int f_0(k)\,\mathrm{d}k, \\ S(f(x)) &= \int f(k)\log[f(k)]\,\mathrm{d}k. \end{aligned}\right\} \tag{11}$$

This function depends in a simple way on the length scale L, of the pattern $f(x)$ as

$$S(f(Lx)) = S(f(x)) + \delta \log L, \tag{12}$$

where δ is the dimension of the Fourier transform. For two patterns with the same basic length scale, a larger value of S indicates a more disordered pattern. In fig. 24 (*b*), we plot $S(f(x))$ against $\log(\langle a^{1/2}\rangle)$ for the froth. For moderate length scales (late times) we observe (with some scatter due to poor statistics) the expected linear relationship since $L \propto \langle a^{1/2}\rangle$. At short length scales (early times), $S(f(x))$ lies below the extrapolated line, indicating that the disorder of the pattern is increasing. As expected, the entropy reaches equilibrium at approximately the same time as other measures of the disorder. At very long times the entropy rises abruptly above the extrapolated line. Most of this rise is due to non-monotonic fluctuations in the measured average bubble radius (fig. 25) at long times and does not represent a real change in the rate of entropy growth. If we plot instead $S(f(x))$ against time (fig. 24 (*a*)), we see a smooth increase in entropy, with a large slope during equilibration when the pattern is increasing in disorder and a smaller constant slope at long times when the pattern is merely increasing in length scale.

Fig. 24

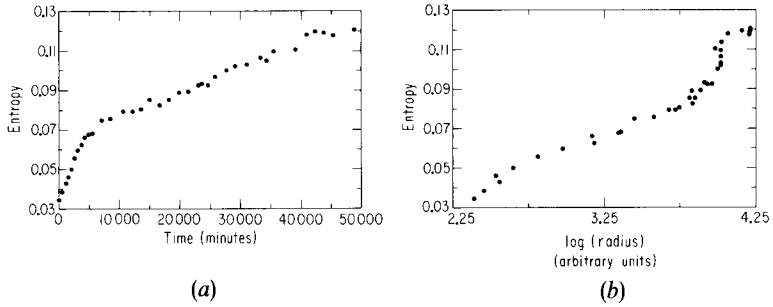

(*a*) (*b*)

Spectral entropy as a function of (*a*) time for the soap froth and (*b*) the logarithm of the mean bubble radius for the froth.

Fig. 25

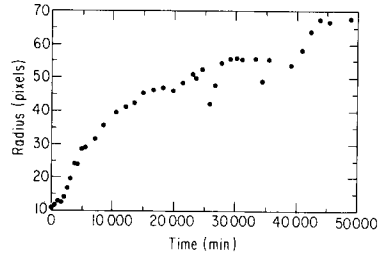

Mean bubble radius as a function of time for the soap froth. Note the non-monotonic scatter at long times owing to edge effects.

Fig. 26

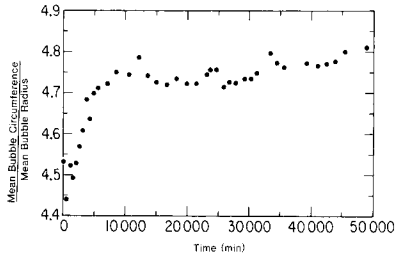

Ratio of the mean bubble circumference to mean bubble radius as a function of time for the soap froth. The ratio reaches a constant value at around 8000 min, when the soap froth reaches its scaling state.

A disadvantage of the entropy method is its sensitivity to noise due to our difficulty in accurately measuring the average length scale of the pattern. However, its general applicability to arbitrary complex patterns makes it a technique worth developing further.

Another technique to examine the stationarity of the pattern is to measure the ratio of the mean bubble circumference to mean bubble radius as a function of time. We plot the soap froth's ratio as a function of time in fig. 26. The ratio reached its equilibrium value of $4{\cdot}73 \pm 0{\cdot}4$ after approximately 8000 min, agreeing with our other measures of system equlibration.

§ 8. Conclusions

The basic agreement between the Potts model and the two-dimensional soap froth is excellent. The Potts model is able to reproduce reasonable distribution functions and nearly perfect correlation functions. In all points it does as well or better than any other model for which we have data, but there are a variety of subtle discrepancies which point in the direction of more fundamental issues. The early-time behaviour of the model differs from that of the froth. The model's hexagonal bubbles are more stable than the froth's. Does this represent a finite-size effect from the coarse graining of the lattice or does it represent a fundamental difference in the way that six-sided bubbles are affected by side redistribution? In the scaling state the tail of the side distribution is longer in the model than in the froth. Clearly this is because, in the model, many-sided bubbles lose sides more slowly than in the froth and presumably gain sides more frequently. Why? Side redistribution is biased against adding to many-sided bubbles in

the soap froth. The Potts model does not seem to have such a correlation. Is this a finite time effect (a bubble cannot see all its sides when it is deciding whether to gain or lose a side because diffusion times along the boundaries are so slow), or is it an anisotropy effect (vertices sink curvature so that the curvature mismatch of many-sided bubbles is partially screened, i.e. many-sided bubbles behave as if they had fewer sides than they really do)? Perhaps the anticorrelation is not intrinsic to ideal grain growth at all but results from nonlinear energy terms which produce anomalous angles in the soap froth (Weaire 1990, Weaire and Bolton 1990). Further investigations are needed to answer this intriguing possibility.

Acknowledgments

This work was partially supported by National Science Foundation Grant DMR-83-16204 and partially by Exxon Research and Engineering. J.A.G. acknowledges support from the Grainger Foundation and Professor Albert Libchaber. We are grateful for many helpful conversations with D. Weaire, N. Rivier, P. Molho and B. Berge and thank S. Matras and M. Luton for their assistance in digitizing the soap froth microstructures.

Note added in proof: Glazier, Srolovitz, Grest and Holm (1990, unpublished) have recently demonstrated that in the zero-anistropy limit, the scaling state distribution functions of the Potts model simulations agree exactly with those of the soap froth. In particular, all the moments increase with increasing anisotropy.

References

Aboav, D. A., 1970, *Metallography*, **3**, 383.

Anderson, M. P., 1986, *Annealing Processes—Recovery, Recrystallization and Grain Growth, Proceeding of the Seventh Risø International Symposium on Metallurgy and Materials Science*, edited by N. Hansen, D. J. Jensen, T. Leffers and B. Ralph (Risø: Risø National Laboratory), p. 15–34.

Anderson, M. P., Grest, G. S., and Srolovitz, D. J., 1986, *Computer Simulation of Microstructural Evolution*, edited by D. J. Srovlovitz (Warrendale, Pennsylvania: Metallurgical Society of AIME), pp. 77–93; 1989, *Phil. Mag.* B, **59**, 293.

Anderson, M. P., Srolovitz, D. J., Grest, G. S., and Sahni, P. S., 1984, *Acta metall.*, **32**, 783.

Atkinson, H. V., 1988, *Acta metall.*, **36**, 469.

Beck, P. A., 1954, *Adv. Phys.*, **3**, 245.

Beenakker, C. W. J., 1986, *Phys. Rev. Lett.*, **57**, 2454; 1987, *Physica* A, **147**, 256; 1988, *Phys. Rev.* A, **37**, 1697.

Blanc, M., and Mocellin, A., 1979, *Acta metall.*, **27**, 1231.

Crain, I. K., 1978, *Comput. Geosci.*, **4**, 131.

de Almeida, R. M. C., and Iglesias, J. R., 1988, *J. Phys.* A, **21**, 3365.

Enomoto, Y., Kawasaki, K., and Nagai, T., 1989, *Int. J. mod. Phys.* B, **3**, 163.

Feltham, P., 1957, *Acta metall.*, **5**, 97.

Fradkov, V. E., Kravchenko, A. S., and Shvindlerman, L. S., 1985a, *Scripta metall.*, **19**, 1291.

Fradkov, V. E., Shvindlerman, L. S., and Udler, D. G., 1985b, *Scripta metall.*, **19**, 1285; 1987, *Phil. Mag. Lett.*, **55**, 289.

Fradkov, V. E., Udler, D. G., and Kris, R. E., 1988, *Phil. Mag. Lett.*, **58**, 670.

Frost, H. J., and Thompson, C. V., 1986, *Computer Simulation of Microstructural Evolution*, edited by P. J. Srolovitz (Warrendale, Pennsylvania: Metallurgical Society of AIME), pp. 33–47; 1987, *Acta metall.*, **35**, 529.

Frost, H. J., Thompson, C. V., Howe, C. L., and Whang, J., 1988, *Scripta metall.*, **22**, 65.

Fu, T.-L., 1986, M.S. Thesis, Trinity College, Dublin.

Fullman, R. L., 1952, *Metal Interfaces* (Metals Park, Ohio: American Society for Metals), pp. 179–207.

GLAZIER, J. A., 1989, Ph.D. Thesis, University of Chicago.
GLAZIER, J. A., GROSS, S. P., and STAVANS, J., 1987, *Phys. Rev.* A, **36,** 306.
GLAZIER, J. A., and STAVANS, J., 1989, *Phys. Rev.* A, **40,** 7398.
GREST, G. S., ANDERSON, M. P., and SROLOVITZ, D. J., 1986, *Computer Simulation of Microstructural Evolution*, edited by D. J. Srolovitz (Warrendale, Pennsylvania: Metallurgical Society of AIME), pp. 21–32.
GREST, G. S., SROLOVITZ, D. J., and ANDERSON, M. P., 1985, *Acta metall.*, **33,** 509; 1988, *Phys. Rev.* B, **38,** 4752.
KAWASAKI, K., and ENOMOTO, Y., 1988, *Physica* A, **150,** 462.
KAWASAKI, K., NAGAI, T., and NAKASHIMA, K., 1989, *Phil. Mag.* B, **60,** 399.
KIKUCHI, R., 1956, *J. chem. Phys.*, **24,** 861.
LAMBERT, C. J., and WEAIRE, D., 1981, *Metallography*, **14,** 307; 1983, *Phil. Mag.* B, **47,** 445.
LANTEJOUL, C., 1978, *Geometrical Probability and Biological Structures: Buffon's 200th Anniversary*, edited by R. E. Miles and J. Serra (Berlin: Springer), pp. 323–329.
LEWIS, F. T., 1928, *Anat. Rec.*, **38,** 341.
MARDER, M., 1987, *Phys. Rev.* A, **36,** 438.
MILES, R. E., 1974, *Stochastic Geometry*, edited by D. G. Kendall and E. F. Harding (New York: Wiley).
MULLINS, W. W., 1956, *J. appl. Phys.*, **27,** 900; 1986, *Ibid.*, **59,** 1341; 1988, *Scripta metall.*, **22,** 1441.
NAKASHIMA, K., NAGAI, T., and KAWASAKI, K., 1989, *J. statist. Phys.*, **57,** 759.
PLATEAU, J., 1843, *Mem. Acad. R. Belg.*, **16,** 1843, continuing in subsequent issues through 1872 (in French); 1873, *Statique experimentale et theorique des liquides soumis aux seulles forces moleculaires* (Paris: Gauthier-Villars).
RIVIER, N., 1983, *Phil. Mag.* B, **47,** L45; 1985, *Ibid.*, **52,** 795.
SMITH, C. S., 1952, *Metal Interfaces* (Cleveland, Ohio: American Society for Metals), pp. 65–108.
SOARES, A., FERRO, A., and FORTES, M., 1985, *Scripta metall.*, **19,** 1491.
SROLOVITZ, D. J., ANDERSON, M. P., GREST, G. S., and SAHNI, P. S., 1983, *Scripta metall.*, **17,** 241; 1984a, *Acta metall.*, **32,** 1429.
SROLOVITZ, D. J., ANDERSON, M. P., SAHNI, P. S., and GREST, G. S., 1984b, *Acta metall.*, **32,** 793.
SROLOVITZ, D. J., GREST, G. S., and ANDERSON, M. P., 1985, *Acta metall.*, **33,** 2233.
STAVANS, J., and GLAZIER, J. A., 1989, *Phys. Rev. Lett.*, **62,** 1318.
VON NEUMANN, J., 1952, *Metal Interfaces* (Cleveland, Ohio: American Society for Metals), pp. 108–110.
WEAIRE, D., 1974, *Metallography*, **7,** 157; 1990, *Phys. Rev. Lett.*, **64,** 3202.
WEAIRE, D., and BOLTON, J., 1990, *Phil. Mag.* B (submitted).
WEAIRE, D., and KERMODE, J. P., 1983a, *Phil. Mag.* B, **47,** L29; 1983b, *Ibid.*, **48,** 245.
WEAIRE, D., WEJCHERT, J., 1986, *Computer Simulation of Microstructural Evolution*, edited by D. J. Srolovitz (Warrendale Pennysylvania: Metallurgical Society), pp. 49–60.
WEJCHERT, J., WEAIRE, D., and KERMODE, J. P., 1986, *Phil Mag.* B, **53,** 15.